Chapter 6

Simulations of spectra and spin relaxation

1 Simulations of two-spin spectra

We have simulated the noisy spectra of two-spin systems in order to characterize the sensitivity of the example resonator presented in table 5.3. Simulations had normally distributed noise added to each sampled point of the FID, with the variance of the noise determined by equation (4.50) in the case of spin-locked detection, and equation (4.53) in the case of freely-precessing spins. The value

$$A_{\text{det}} = 16$$

was used to characterize noise in the motion detector, as in the measurements reported in reference [25]. This value of A_{det} renders the spin noise negligible in comparison to instrument noise. For detection of freely-precessing spins, resonator-induced relaxation was included in the simulation by writing GAMMA programs [39] which simulated the motion of the spin system under the reduced master equation (2.17). For spin-locked detection using the scheme described in section 1 of chapter 5, no relaxation was included in the simulation. (This detection scheme measures a single point $\langle I_x(t_1)\rangle$ of the FID with each shot of the measurement, and the spins are off resonance from the mechanical oscillator until time t_1.) We assumed that transverse decay of a two-spin system in a lattice at 10 mK would be negligible during the range

of values t_1 sampled during spin-locked measurements, which included times up to 3 s after the beginning of the FID. As in the optimization described in section 6 of chapter 5, we used

$$T_{1\rho} = 1\,\mathrm{s}\,,$$

rather than assuming that resonator-induced relaxation was responsible for the decay of the spin-locked signal, which would have yielded

$$T_{1\rho} = 2/R_h = 1.5\,\mathrm{s}\,.$$

1.1 Noninteracting spins

For a system of two noninteracting spins coupled to the mechanical resonator, the discussion of section 5 of chapter 3 suggests that a chemical-shift difference of

$$\delta\omega/2\pi = 200\,\mathrm{Hz}$$

would yield the same time constant for resonator-induced transverse relaxation of the freely precessing dipole that would be observed for a single spin:

$$2/R_h = 1.5\,\mathrm{s}\,.$$

Under these conditions, section 6 of chapter 4 shows that detection of the freely precessing transverse dipole is more sensitive than spin-locked detection, particularly if the lifetime of the spin-locked signal is shortened from $2/R_h$ to 1 s. Indeed, equations (4.50) and (4.56) predict that under these conditions, detection of freely-precessing spins will be more sensitive than spin-locked detection by a factor of about 1.75. Figures 6.1 and 6.2 are consistent with this prediction, since the peaks at 100 Hz and 300 Hz stand out more sharply from the noise in the case where the freely-precessing spins drive the magnet than in the case of spin-locked detection.

Each of these spectra requires 32,000 transients. In estimating the time required to obtain the spectra, note first that the time constant for resonator-induced longi-

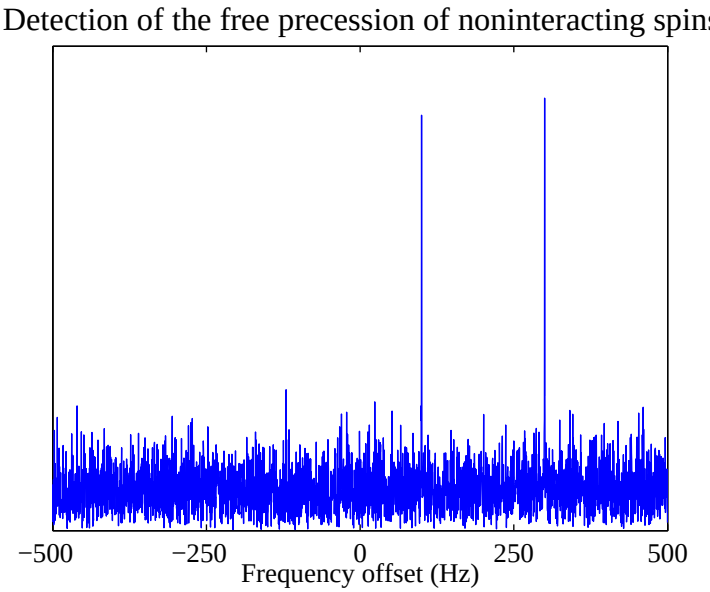

Figure 6.1: Simulated spectrum of two noninteracting spins detected without spin-locking. The spin Hamiltonian is $H = (100\,\mathrm{Hz})\,I_{1z} + (300\,\mathrm{Hz})\,I_{2z}$. Transverse relaxation induced by the example resonator of table 5.3 is included in the simulation of the noiseless FID, and normally distributed instrument noise associated with detection by the same resonator is added to the FID. Thermal polarization is assumed at the beginning of each transient. The acquisition time is $\sim 50\,\mathrm{h}$.

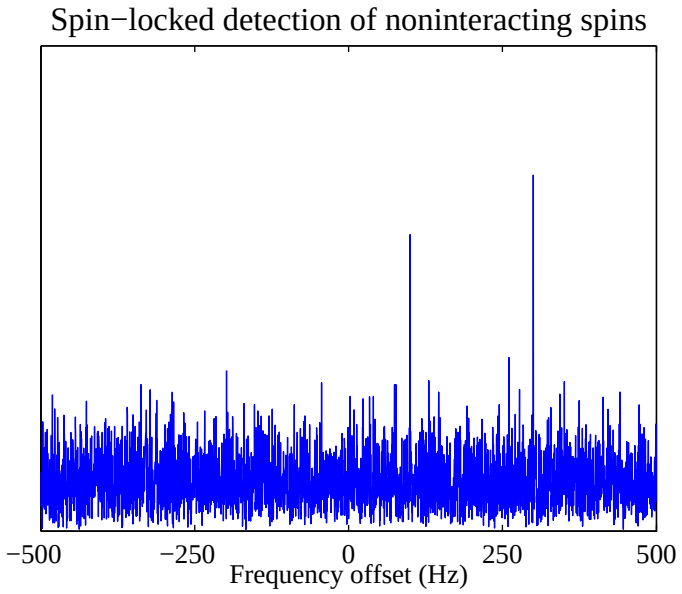

Figure 6.2: Simulated spectrum of two noninteracting spins detected with spin-locking, with $T_{1\rho} = 1\,\mathrm{s}$. The spin-resonator system is the same as in figure 6.1, but resonator-induced transverse relaxation is eliminated from the simulation. Acquisition time for the spectrum is $\sim 60\,\mathrm{h}$. Figures 6.1 and 6.2 are consistent with the prediction that for this system, detection of freely-precessing spins is more sensitive than spin-locked detection by a factor of about 1.75.

tudinal relaxation between transients is

$$1/R_h = 0.77\,\mathrm{s}\,, \tag{6.1}$$

and we estimate the relaxation time between transients as $3/R_h = 2.3\,\mathrm{s}$, for consistency with the assumption that thermal polarization is present at the beginning of each transient. For both figures, the detection period for a single transient lasts 3 s. In the case where freely precessing magnetization is detected, this is twice the time constant $2/R_h$ for resonator-induced transverse relaxation (chosen after experimenting with simulated FIDs of different lengths in order to produce peaks clearly differentiated from the noise), while in the case of spin-locked detection, this is $3T_{1\rho}$ (an assumed value for the protocol used to analyze the resonator's detected mechanical motion). The acquisition time for figure 6.1 is therefore

$$(2.3\,\mathrm{s} + 3\,\mathrm{s}) \times 32000 \approx 50\,\mathrm{h}\,.$$

For the spin-locked detection simulated in figure 6.2, an initial period of free precession which precedes the detection period is also required, and the average length of this period is 1.5 s, which gives an acquisition time of

$$(2.3\,\mathrm{s} + 3\,\mathrm{s} + 1.5\,\mathrm{s}) \times 32000 \approx 60\,\mathrm{h}\,.$$

1.2 Vinyl bromide

Reference [40] has studied the structure of dibromoethylene adsorbed on a silicon surface and proposed the two structures shown in figure 6.3. We simulated spin-locked detection of one of these structures, adsorbed vinyl bromide, using the example resonator. Standard bond angles and bond lengths were used to estimate the Hamiltonian for dipolar coupling. A chemical shift difference was incorporated into the Hamiltonian by using the value 0.6 ppm given in the literature for vinyl bromide

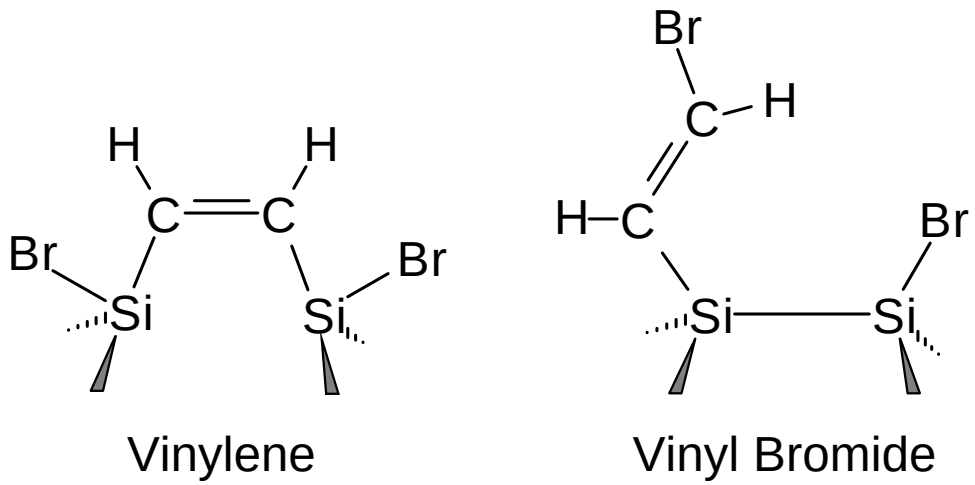

Figure 6.3: Two possible structures for dibromoethylene adsorbed on a silicon surface, proposed by reference [40].

in deuterated dichloromethane [41]. The spin Hamiltonian obtained in this way is

$$H_{\text{vinyl bromide}} = (0.6)\,(628\,\text{Hz})\,I_{z,1} + (1840\,\text{Hz})\,(2I_{z,1}I_{z,2} - I_{x,1}I_{x,2} - I_{y,1}I_{y,2})\,.$$

Figure 6.4 shows the simulated spectrum, for which the acquisition time is $\sim 60\,\text{h}$, as in figure 6.2. Since the dipolar coupling is sensitive to variations in geometry such as those shown in figure 6.3, this simulation suggests the possibility of chemical studies in which NMR spectroscopy is used with single-spin sensitivity.

2 Simulations of spin relaxation

Chapter 3 analyzes resonator-induced spin relaxation in samples containing more than one spin. Here we present GAMMA simulations [39] which illustrate and extend the results obtained in that section. The resonator used for these simulations has parameters similar to those given in table 5.3, although simplifications have been made to facilitate the interpretation of the graphs. For simulations of spin relaxation, the rate constant for spontaneous emission is $R_0 = 1\,\text{s}^{-1}$, the Larmor frequency has a magnitude of 600 MHz, and the temperature is approximately zero Kelvins, i.e., we

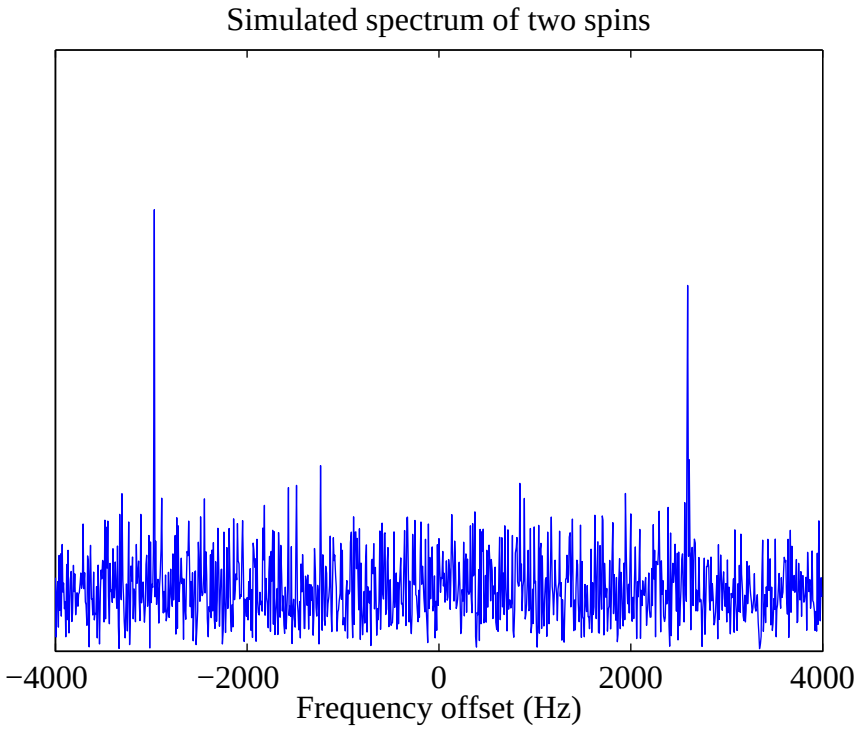

Figure 6.4: Simulated spectrum of a single molecule of adsorbed vinyl bromide, detected with spin-locking. The FID contains 1024 sampled complex points, averaged during 32,000 transients. Thermal polarization is assumed at the beginning of each transient. Acquisition time for this spectrum is $\sim 60\,\mathrm{h}$.

have set $n_{\text{th}} < 10^{-4}$ in equation (2.17). The interaction frame used for simulations of the relaxation of $\langle I_x \rangle$ is defined as follows: the interaction-frame reduced density matrix for the spins $\rho_s(t)$ is found by evolving the spin system forward in time for a period t from the initial state $\rho_s(0)$ using the full evolution superoperator corresponding to equation (2.17), and then evolving the spins backward in time for the same period using the superoperator for evolution under the full spin Hamiltonian without relaxation.

2.1 Relaxation of noninteracting spins

Figure 6.5 presents the results of two simulations performed in order to test the estimate (3.21) of the time T_{trap} required for an initially disordered system to approach its spin-trapped equilibrium state:

$$T_{\text{trap}} = \frac{1}{R_0 \sqrt{N/2}}.$$

Note that T_{trap} also characterizes the time required for resonator-induced spin-spin correlations to develop, and it can be used to estimate the frequency at which indirect spin-spin torques must be modulated if spin trapping is to be suppressed. The solid and dashed curves show the relaxation of two systems of noninteracting spins which all experience the same field while relaxing from an initially disordered state, with the respective systems having $N = 144$ and $N = 36$ spins. The curves are normalized to take the value 1 when a system has relaxed to its spin-trapped equilibrium state. Figure 6.5 suggests that (3.21) works reasonably well as an estimate of the characteristic time required for $\langle I_z \rangle$ to approach its equilibrium value. For both curves, the time $t = T_{\text{trap}}$ corresponds to a point at which the system has relaxed to about 70% of its spin-trapped polarization.

The semiclassical model used to estimate T_{trap} suggests that chemical-shift offsets could reverse the sign of indirect spin-spin torques, thereby allowing resonator-induced relaxation to be characterized by a rate constant, and the simulations shown in figures 6.6 through 6.9 are consistent with this hypothesis. In figures 6.6 and 6.7, the

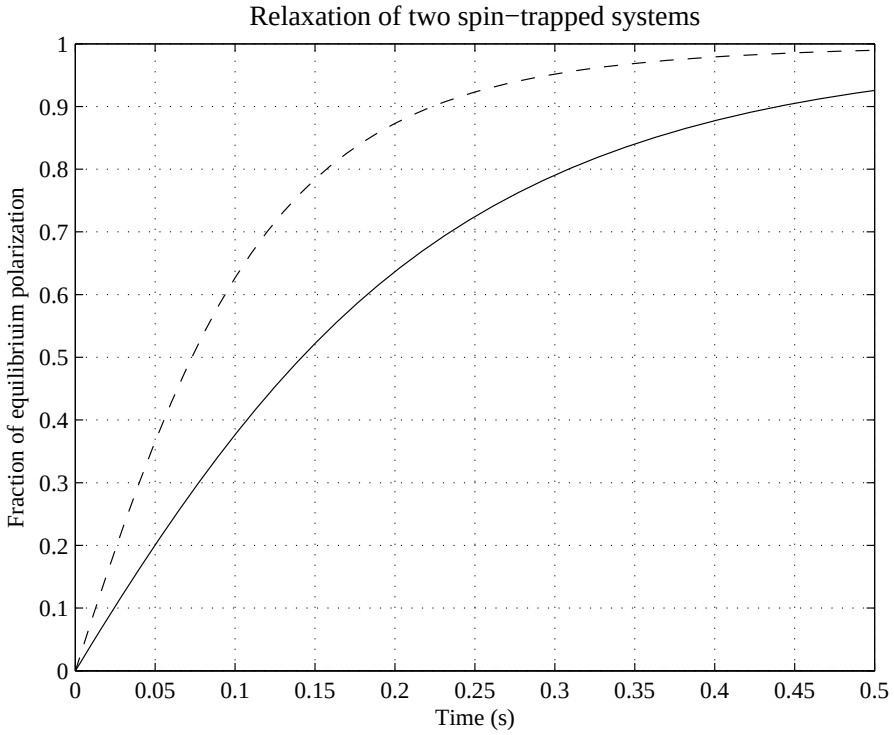

Figure 6.5: The solid and dashed curves show the respective relaxation of noninteracting systems having $N = 36$ and $N = 144$, with $R_0 = 1\,\mathrm{s}^{-1}$. The curves are normalized to take the value 1 when a system has relaxed to its spin-trapped equilibrium state. For each curve, the time $t = \left(R_0\sqrt{N/2}\right)^{-1}$ corresponds to a point at which the system has relaxed to about 70% of its spin-trapped polarization.

spins are initially aligned along the x-axis. The dashed curves show resonator-induced longitudinal and transverse relaxation, while the solid curves show the ideal longitudinal and transverse relaxation which would be observed if the relaxation were exponential with the respective rate constants R_0 and $R_0/2$ that govern the relaxation of an isolated spin interacting with the resonator. The dotted curve in each figure displays the evolution of $\left\langle N/2 - I_x^2 - I_y^2 \right\rangle$. Since the relaxation equation for $\langle I_z \rangle$ can be expressed as

$$\frac{d}{dt}\langle I_z \rangle = -R_h \left\{ \langle I_z \rangle - \frac{N/2}{2\langle n_{\rm th} \rangle + 1} \right\} - R_0 \left\langle N/2 - I_x^2 - I_y^2 \right\rangle ,$$

a plot of $\left\langle N/2 - I_x^2 - I_y^2 \right\rangle$ displays the instantaneous contribution of indirect spin-spin torques to longitudinal relaxation. Adding chemical shift offsets spaced in steps of 1 Hz causes the indirect spin-spin torques to be modulated quickly enough that the contribution of these torques to the relaxation is effectively suppressed, and the simulated relaxation closely follows the exponential curves.

Figures 6.8 and 6.9 show longitudinal relaxation from a completely disordered initial state. Note that in figure 6.9, the spacing of chemical shift frequencies in steps of 1 Hz is sufficient to suppress completely the contribution of the indirect torques to longitudinal relaxation. The value of $\left\langle N/2 - I_x^2 - I_y^2 \right\rangle$, which shows the instantaneous contribution of indirect spin-spin torques, oscillates without ever becoming large enough to affect the relaxation substantially. By way of contrast, the same spacing of chemical shift frequencies leaves noticeable wiggles in the simulated curves of figure 6.7, and $\left\langle N/2 - I_x^2 - I_y^2 \right\rangle$ initially oscillates between much larger values. These differences can be rationalized by noting that when the spins are initially disordered, the indirect torques do not add coherently, and modulation of these torques during a period of one or two seconds is sufficient to suppress their contribution to longitudinal relaxation. In the case where the spins are initially aligned along the x-axis, the indirect torques add coherently, and the effect of these torques can be seen even when their contribution is modulated within a similar time period.

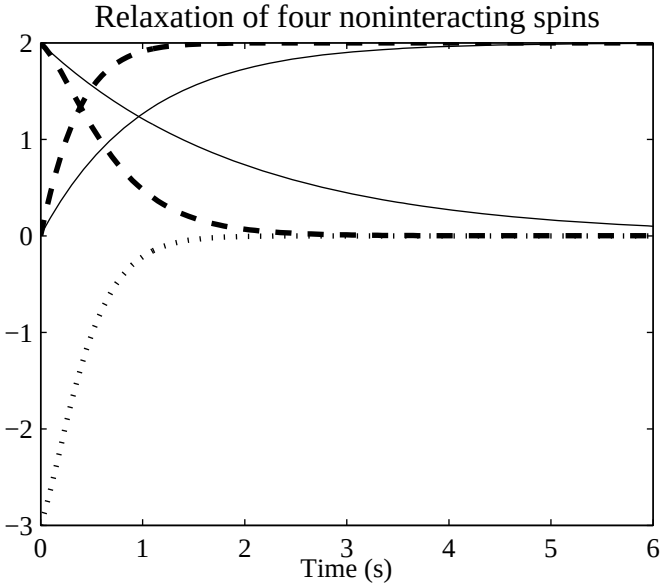

Figure 6.6: Relaxation of four isochronous spins which are initially aligned along the x-axis. The dashed curves show the simulated relaxation of $\langle I_x \rangle$ and $\langle I_z \rangle$, while the solid curves show ideal exponential longitudinal and transverse relaxation with respective time constants $1/R_0$ and $2/R_0$. The dotted curve shows the evolution of $\langle N/2 - I_x^2 - I_y^2 \rangle$, which determines the instantaneous contribution of indirect spin-spin torques to longitudinal relaxation.

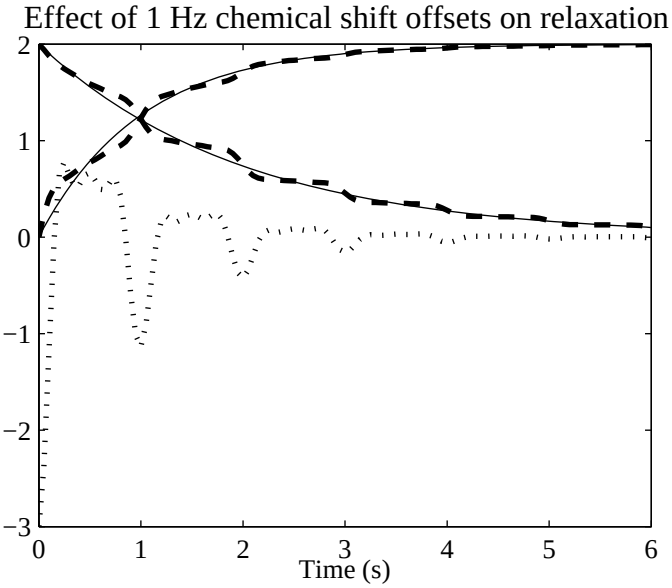

Figure 6.7: Adding chemical shift offsets spaced in steps of 1 Hz causes the indirect spin-spin torques to be modulated quickly enough that their contribution to relaxation is effectively suppressed.

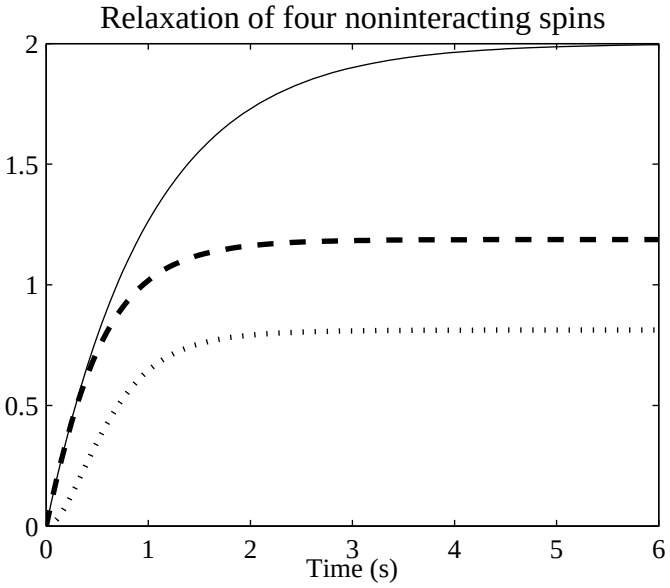

Figure 6.8: Relaxation of four noninteracting spins which experience the same field and are initially completely disordered. The dashed curve shows the simulated relaxation of $\langle I_z \rangle$, while the dotted curve shows the evolution of $\langle N/2 - I_x^2 - I_y^2 \rangle$. The solid curve shows exponential longitudinal relaxation with time constant $1/R_0$.

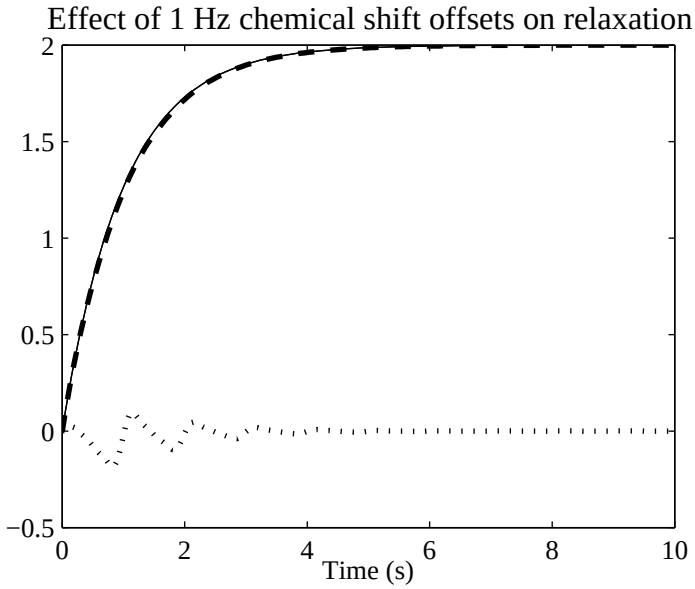

Figure 6.9: Adding chemical shift offsets spaced in steps of 1 Hz causes the indirect spin-spin torques to be modulated quickly enough that their contribution to relaxation is completely suppressed, and the simulated curve closely follows the ideal exponential curve.

2.2 Relaxation of dipole-dipole coupled spins

Figures 6.10, 6.11, and 6.12 show GAMMA simulations of the relaxation of four-spin systems coupled by the dipolar Hamiltonian. The spin Hamiltonian for these simulations has the form

$$\begin{aligned} H &= \omega_0 I_z + H_D, \\ H_D &= \sum_{i>j} \omega_{ij} \left(3 I_{z,i} I_{z,j} - \mathbf{I}_i \cdot \mathbf{I}_j\right). \end{aligned} \tag{6.2}$$

In these figures, the dotted curve corresponds to a system in which the dipolar coupling was eliminated by choosing $\omega_{ij} = 0$ for all i, j. The system characterized by the dash-dot curve has a Hamiltonian obtained by letting each $\omega_{ij}/2\pi$ be randomly chosen, with a flat probability distribution between 1 kHz and 2 kHz. The Hamiltonian yielding the dash-dash relaxation curves was obtained by broadening the distribution of $\omega_{ij}/2\pi$ to lie between 0 Hz and 2 kHz. The solid curves show ideal exponential relaxation with the rate constants for longitudinal relaxation and transverse relaxation given by R_0 and $R_0/2$, respectively.

Longitudinal relaxation of an initially disordered system is shown in figure 6.10. The dipole-dipole coupled systems show two different time scales for relaxation, with a short initial period of fast relaxation being followed by a longer period of slow relaxation. Extending the simulations to $t = 150$ s shows that the systems effectively remain trapped away from the ground state.

This behavior can be rationalized using results obtained in section 4 of chapter 3 for a system of three dipole-dipole coupled spins. The rules for addition of angular momenta allow a collection of three spins 1/2 to be represented as a single particle with $I = 3/2$ and two particles with $I = 1/2$. Equations (3.28) and (3.29) show that one of the $I = 1/2$ particles (or "manifolds") can be defined in such a way that its two states $|1/2, +\rangle$, $|1/2, -\rangle$ are eigenstates of H_D. As the spins interact with the cold mechanical resonator, the combined population of this manifold will be transferred to the lower-energy state $|1/2, +\rangle$ within a time period of order R_0 and then remain

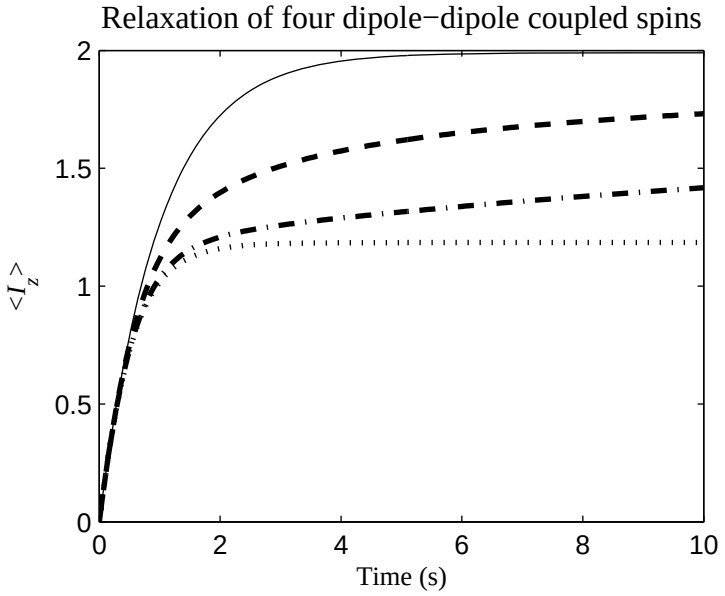

Figure 6.10: Longitudinal relaxation of four dipole-dipole coupled spins from an initially disordered state. For the dash-dot curve, the dipolar Hamiltonian was obtained by letting the frequencies $\omega_{ij}/2\pi$ of equation (6.2) be randomly chosen, with a flat probability distribution between 1 kHz and 2 kHz. For the the dash-dash curve, the frequencies $\omega_{ij}/2\pi$ were randomly selected between 0 Hz and 2 kHz. For purposes of comparison, the solid curve shows exponential relaxation with time constant $1/R_0$, and the dotted curve shows the relaxation of a system of noninteracting spins.

in that state indefinitely. Table 3.1 shows that H_D does not strongly couple the remaining $I = 1/2$ manifold with the $I = 3/2$ manifold unless the magnitudes of the dipolar couplings are well separated. When the coupling between angular momentum manifolds is weak, two different time scales of relaxation are expected. An initial period of fast relaxation occurs as population is transferred to the lowest-energy state of each manifold, and this is followed by a period of slow relaxation as population is slowly transferred to the $I = 3/2$ manifold and then relaxes to the ground state of the spin system. Simulated relaxation of three-spin systems confirms these expectations.

The four-spin simulations of figure 6.10 can be rationalized by the hypothesis that the relaxation is governed by similar processes. The systems appear to relax quickly from a disordered state to a state in which the population of each manifold is in the manifold's ground state. Relaxation out of this trapped state occurs on a slower time scale as population is transferred between manifolds with different values of I. In figure 6.10, the efficiency of transfer between manifolds of different I separates the three simulated curves after an initial period in which they relax at the same rate. Extending the simulation to $t = 150\,\mathrm{s}$ suggests that the systems represented by the dash-dash curve and the dash-dot curve effectively become trapped away from the ground state. A system of four spins 1/2 yields one $I = 2$ manifold, three $I = 1$ manifolds, and two $I = 0$ manifolds. The dash-dash curve can be rationalized by the hypothesis that population is trapped in the two $I = 0$ manifolds, while the dash-dot curve can be rationalized by the hypothesis that population is trapped in the two $I = 0$ manifolds and one of the $I = 1$ manifolds. Both curves become flat at a value a fraction of a percent below the trapped value predicted by these hypotheses.

The discussion in section 5 of chapter 3 analyzes the way in which the resonator can induce fast transverse relaxation in a system of two or more spins. A coherence ρ_{ab} between states $|a\rangle$ and $|b\rangle$ can be disrupted when the system makes a transition away from one of these states. Transitions do not necessarily decrease the order within a system, however. A transition from $|a\rangle$ to $|c\rangle$ might replenish a coherence ρ_{cb} at the same time that it depletes ρ_{ab}, leaving the sum $\rho_{ab} + \rho_{cb}$ unchanged. If a perturbation changes the frequency of ρ_{ab} or ρ_{cb} so that their relative phase varies

during the time needed for non-negligible transfer from ρ_{ab} to ρ_{cb}, however, then transfer from ρ_{ab} to ρ_{cb} depletes ρ_{ab} without replenishing ρ_{cb}, since the terms added to ρ_{cb} during different time steps interfere destructively. An addition to the spin Hamiltonian which perturbs the degeneracies of distinct coherences can therefore transform reversible transfer between coherences into irreversible decay, and in this way modify the rate of resonator-induced transverse relaxation. In section 5 of chapter 3, this was illustrated using analytic expressions for the transverse decay of two-spin systems.

Figure 6.11 shows that the presence of dipolar couplings can substantially accelerate transverse relaxation in a four-spin system. The solid curve shows ideal exponential relaxation with time constant

$$2/R_0 = 2\,\mathrm{s}\,,$$

and the dotted curve shows the simulated relaxation of a system of four noninteracting isochronous spins. Addition of the dipolar Hamiltonian H_D increases the relaxation rate, with the magnitude of the change depending on the spacing of the frequencies ω_{ij} which appear in (6.2). The fast transverse relaxation induced by the resonator in these examples would significantly decrease the sensitivity of a scheme which detects freely precessing spins

The tendency of the dipolar Hamiltonian H_D to accelerate transverse relaxation cannot be interpreted as radiation damping, which is associated with rotation of a sample dipole rather than true decay. This is demonstrated by figure 6.12, which shows the longitudinal relaxation of four-spin systems having the spins initially aligned with the x-axis. The dotted curve shows longitudinal relaxation in the absence of H_D, while the dash-dash curve corresponds to the same Hamiltonian H_D as the dash-dash curves in figures 6.10 and 6.11. The solid curve shows exponential relaxation with a time constant $1/R_0$. "Turning on" the dipolar coupling slows down longitudinal decay at the same time that it accelerates transverse decay; hence, it is not associated with simple rotation of the sample dipole.

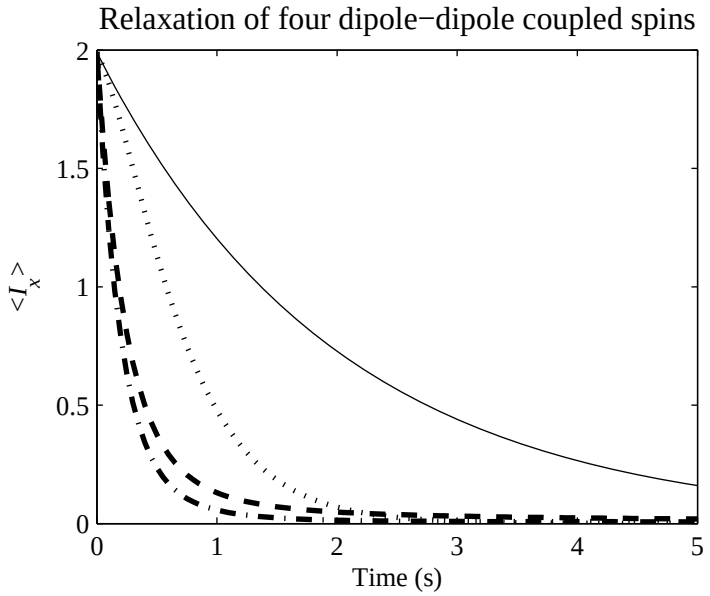

Figure 6.11: Transverse relaxation of four dipole-dipole coupled spins which are initially aligned with the x-axis. For the dash-dot curve, the dipolar Hamiltonian was obtained by letting the frequencies $\omega_{ij}/2\pi$ of equation (6.2) be randomly chosen, with a flat probability distribution between 1 kHz and 2 kHz. For the dash-dash curve, the frequencies $\omega_{ij}/2\pi$ were randomly selected between 0 Hz and 2 kHz. For purposes of comparison, the solid curve shows exponential relaxation with time constant $2/R_0$, and the dotted curve shows the relaxation of a system of noninteracting spins. This figures shows that "turning on" the dipolar interaction can accelerate resonator-induced transverse relaxation.

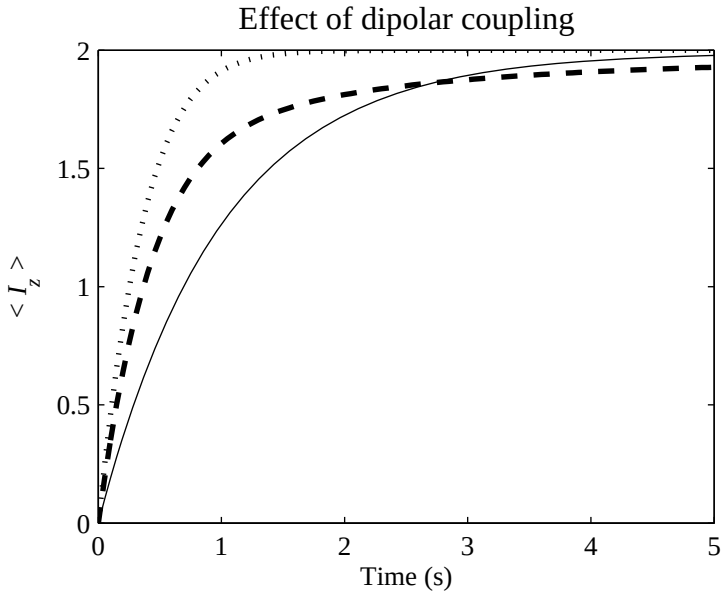

Figure 6.12: Longitudinal relaxation of four-spin systems. The solid curve shows exponential relaxation with time constant $1/R_0$. The dash-dash curve represents a dipole-dipole coupled system, and the dotted curve represents a system of noninteracting spins. "Turning on" the dipolar coupling slows down longitudinal decay.

Figure 6.13 reinforces the distinction between radiation damping and fast transverse relaxation induced by the resonator. In section 5 of chapter 3, we studied transverse relaxation of a two-spin sample having a weak dipolar coupling and a large chemical shift offset between the spins. We showed that the large chemical shift offset guaranteed that longitudinal relaxation would proceed exponentially with time constant $1/R_h$ (or $1/R_0$ in the case where the resonator is at zero Kelvins), while the presence of the dipolar coupling accelerated the transverse relaxation induced by the resonator. Figure 6.13 extends the results of that section by presenting simulated relaxation of a four-spin system which has a chemical-shift offset of $j \times 4000\,\mathrm{Hz}$ added to spin j, in addition to the same dipolar coupling H_D which yielded the dash-dash curves in figures 6.10 through 6.12. For purposes of comparison with the simulation, the longitudinal and transverse relaxation predicted for a single-spin sample is shown using solid curves. Simulated longitudinal relaxation is only slightly perturbed from that of a single spin, while the transverse dipole relaxes in a fraction of the time

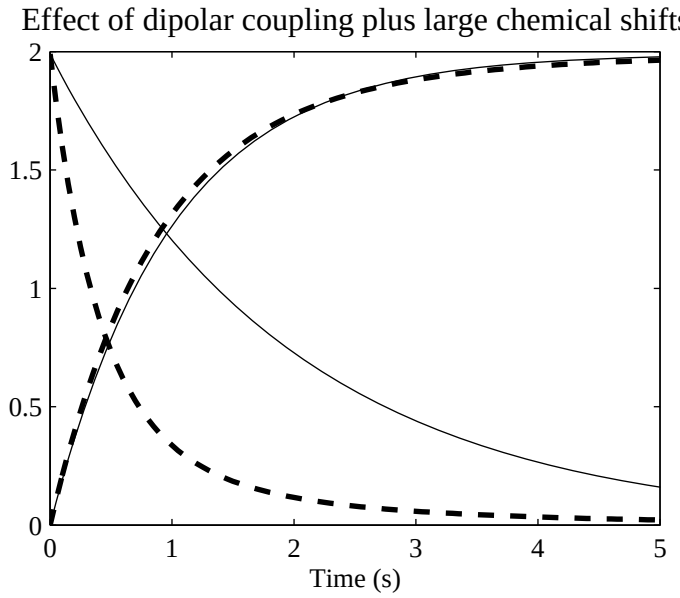

Figure 6.13: Relaxation of a four-spin system which includes dipolar couplings smaller than the spacing of chemical shift offsets. All spins are initially aligned along the x-axis. Solid curves show ideal exponential longitudinal and transverse relaxation with respective time constants $1/R_0$ and $2/R_0$. The dashed curves show the simulated relaxation of $\langle I_x \rangle$ and $\langle I_z \rangle$. The transverse relaxation is accelerated by the presence of the dipolar coupling, while the longitudinal relaxation closely follows the ideal exponential curve, due to the presence of large chemical shift offsets.

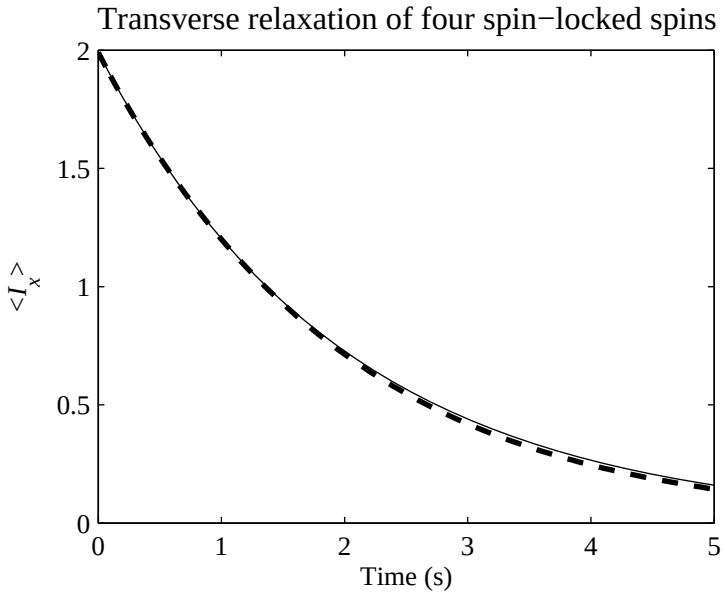

Figure 6.14: Resonator-induced relaxation of a spin-locked sample of four dipole-dipole coupled spins. The solid curve shows the predicted exponential transverse relaxation with time constant $2/R_0$.

required for transverse relaxation of a single spin.

Figure 6.14 illustrates the result (3.35) obtained in section 6 of chapter 3:

$$T_{1\rho} = R_h/2.$$

The dash-dash curve shows simulated relaxation of a spin-locked system of four dipole-dipole coupled spins. The internal spin Hamiltonian is the same dipolar Hamiltonian H_D used for the dash-dash curves in figures 6.10 through 6.12, and $\omega_1/2\pi = 10\,\mathrm{kHz}$. The solid curve shows exponential relaxation with time constant $R_0/2 = R_h/2$. We see from figure 6.14 that spin-locking with a Rabi frequency of 10 kHz is sufficient to average both H_D and the superoperator for resonator-induced relaxation, thereby suppressing the fast transverse relaxation shown in figure 6.11.

The qualitative character of resonator-induced longitudinal relaxation of $N \gg 1$ dipole-dipole coupled spins depends on the efficiency with which the Hamiltonian H_D transfers populations between angular momentum manifolds corresponding to differ-

ent values of I. In the limiting case where transfers between manifolds occur quickly, H_D equalizes the population of all states within a given eigenspace of I_z. Resonator-induced transfers of population to low-energy states within a manifold immediately result in compensating transfers between manifolds as the population of all states within each eigenspace of I_z are equalized. Figures 6.15 and 6.16 present simulations of longitudinal relaxation for this limiting case. The dashed curves show simulations in which population is equalized among all states of each I_z eigenspace at the end of each 0.01 s time step of resonator-induced relaxation. (For these figures, the initial state is completely disordered, and the simulation includes no spin-spin interactions during the time steps.) The solid curves show ideal exponential relaxation with rate constant R_0. In spite of the fact that the number of angular momentum manifolds having small I is vastly greater than the number of manifolds having I near $N/2$ for these systems, the simulations suggest that efficient redistribution within eigenspaces of I_z can result in fast longitudinal relaxation to a polarization near 1.

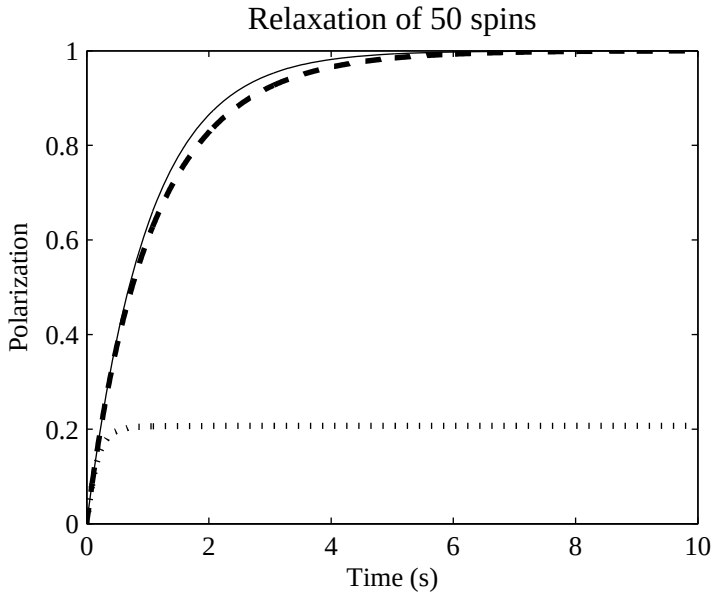

Figure 6.15: Resonator-induced longitudinal relaxation of 50 spins from a disordered state. The dashed curve shows simulated relaxation in the regime where dipolar interactions efficiently redistribute population within each eigenspace of I_z during the relaxation. For purposes of comparison, the dotted curve shows relaxation of noninteracting spins to a trapped state, and the solid curve shows ideal exponential relaxation with time constant $1R_0$.

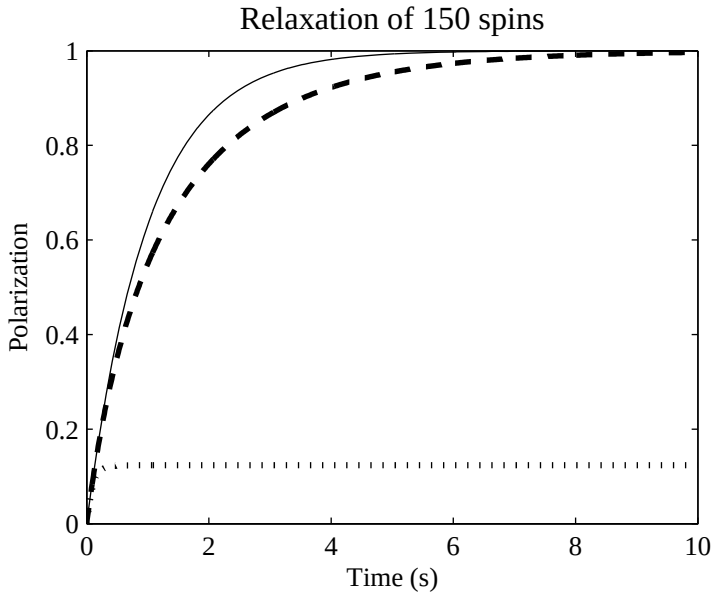

Figure 6.16: Resonator-induced longitudinal relaxation of 150 spins from a disordered state. As in figure 6.15, the dashed curve shows simulated relaxation in the regime where dipolar interactions efficiently redistribute population within each eigenspace of I_z during the relaxation. The dotted curve shows relaxation of noninteracting spins to a trapped state, and the solid curve shows ideal exponential relaxation with time constant $1R_0$.